Supporting Information for

Dynamic Evolution of a Cathode Interphase Layer at the Surface of $LiNi_{0.5}Co_{0.2}Mn_{0.3}O_2$ in Quasi-Solid-State Lithium Batteries

Hui-Juan Guo[†,‡], Huai-Xiang Wang[‡,⊥], Yu-Jie Guo[†,‡], Gui-Xian Liu[†,‡], Jing Wan[†,‡], Yue-Xian Song[†,‡], Xin-An Yang[‡,⊥], Fei-Fei Jia[∥], Fu-Yi Wang[∥,‡], Yu-Guo Guo[†,‡,§], Rui Wen[†,‡,§,*], Li-Jun Wan[†,‡]

[†]CAS Key Laboratory of Molecular Nanostructure and Nanotechnology, and Beijing National Laboratory for Molecular Sciences, CAS Research/Education Center for Excellence in Molecular Sciences, Institute of Chemistry, Chinese Academy of Sciences, Beijing 100190, China.

[‡]University of Chinese Academy of Sciences, Beijing 100049, P. R. China Beijing 100190, China.

[⊥]Laboratory for Advanced Materials and Electron Microscopy, Beijing National Laboratory for Condensed Matter Physics, Institute of Physics, Chinese Academy of Sciences, Beijing, 100190, China.

[∥]CAS Key Laboratory of Analytical Chemistry for Living Biosystems, Beijing National Laboratory for Molecular Sciences, National Centre for Mass Spectrometry in Beijing, Institute of Chemistry, Chinese Academy of Sciences, Beijing, 100190, China.

[§]Dongguan TAFEL New Energy Technology Co., Ltd, Dongguan, 523000, China.

Supplementary Figures

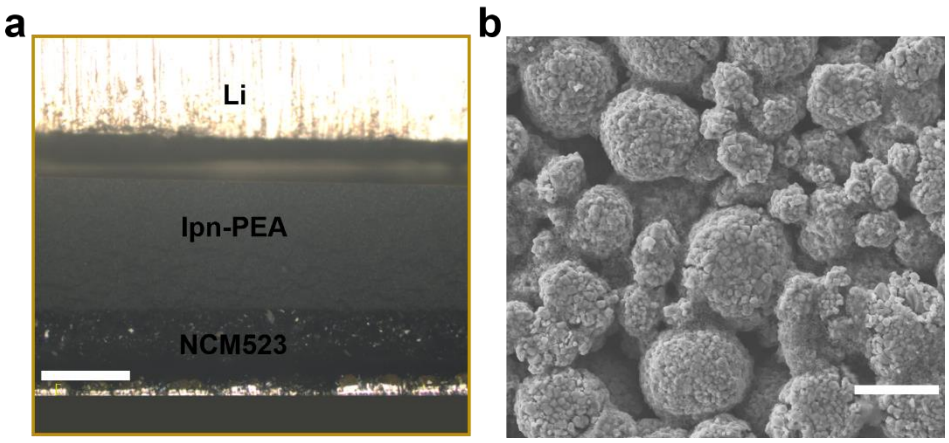

Figure S1. (a) The optical image of the cross-section interface in a NCM523/ipn-PEA/Li cell before cycling. The scale bar is 100 μm. (b) The SEM image of NCM523. The scale bar is 10 μm.

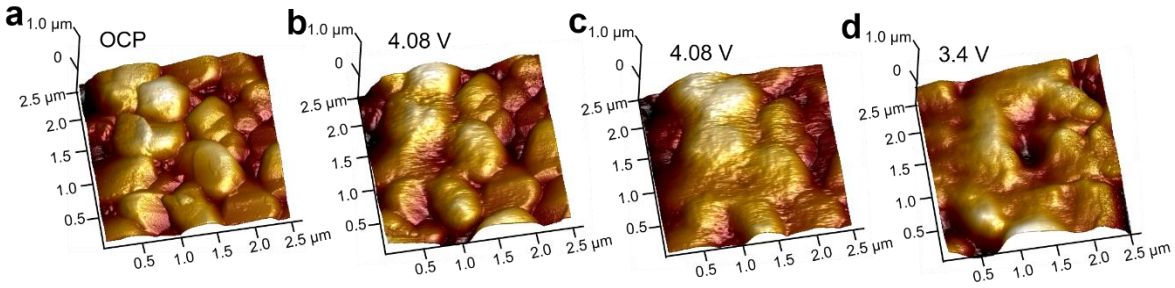

Figure S2. *In situ* 3D AFM images of the morphological evolution of the cathode interphase layer on NCM523 particle surfaces upon charge/discharge. (a) OCP. (b) Charged to 4.08 V for 1 h. (c) Charged to 4.08 V for 2.5 h. (d) Discharged to 3.4 V for 1 h.

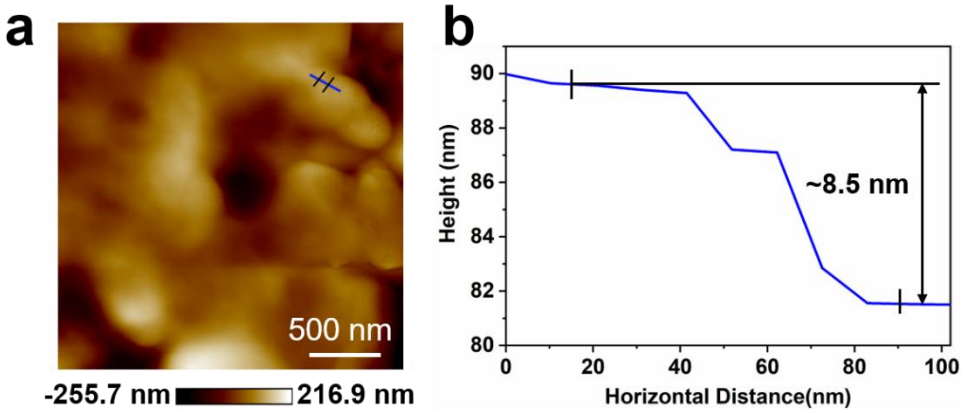

Figure S3. (a) AFM image of NCM523 electrode. (b) The cross-sectional profile along the boundary of the cathode interphase layer measured on (a).

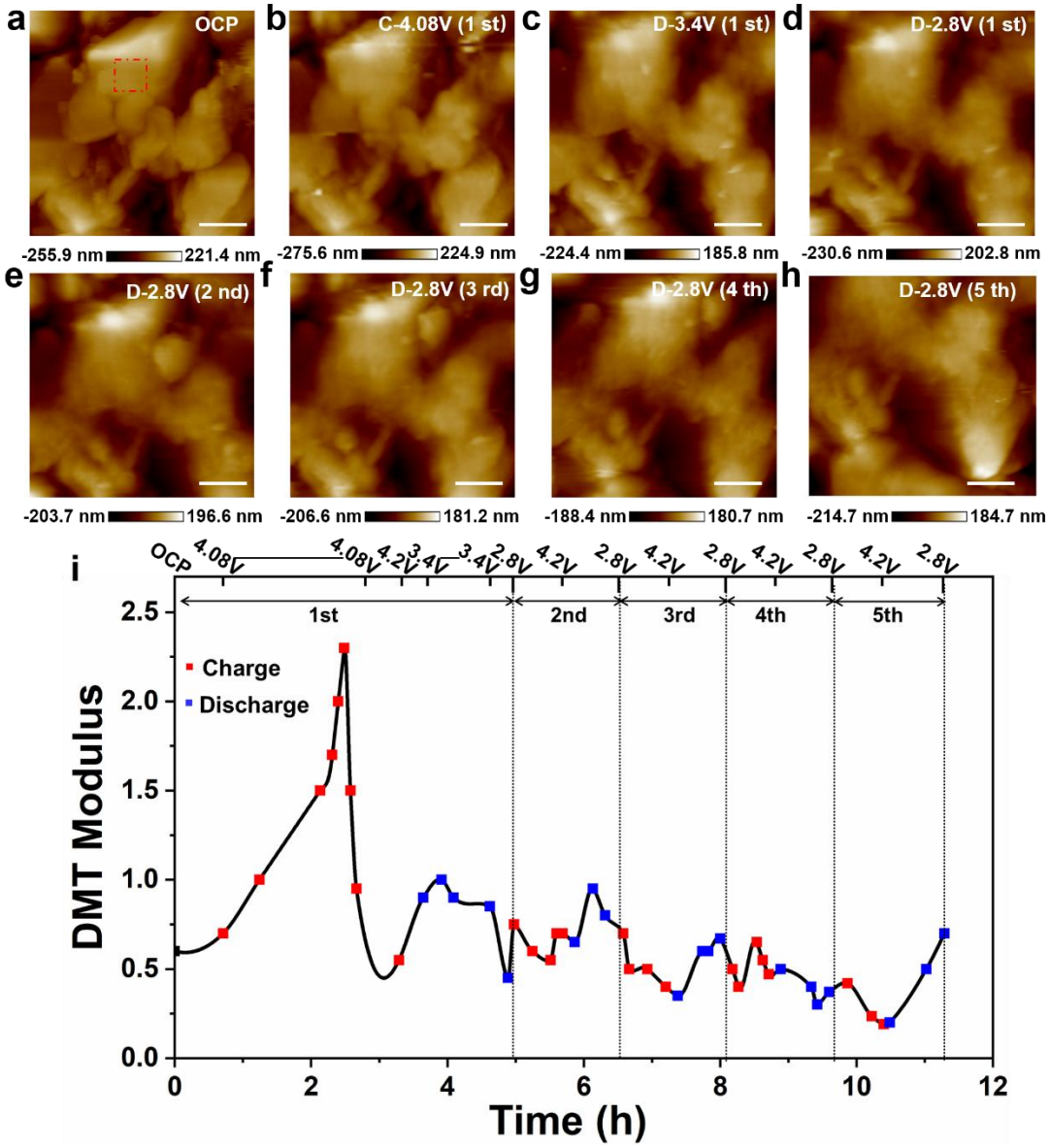

Figure S4. *In situ* AFM images of the NCM523 cathode surface upon 5 cycles. The scale bars are 300 nm. (a) OCP. (b) Charged to 4.08 V for 2.5 h at the first cycle. (c) Discharged to 3.4 V for 1h at the first cycle. (d) Discharged to 2.8 V at the first cycle. (e) Discharged to 2.8 V at the second cycle. (f) Discharged to 2.8 V at the third cycle. (g) Discharged to 2.8 V at the fourth cycle. (h) Discharged to 2.8 V at the fifth cycle. (i) Quantitative measurements of the average DMT modulus of cathode interphase on NCM523 cathode surface at a certain position (red frame in Figure S4a) upon 5 cycles.

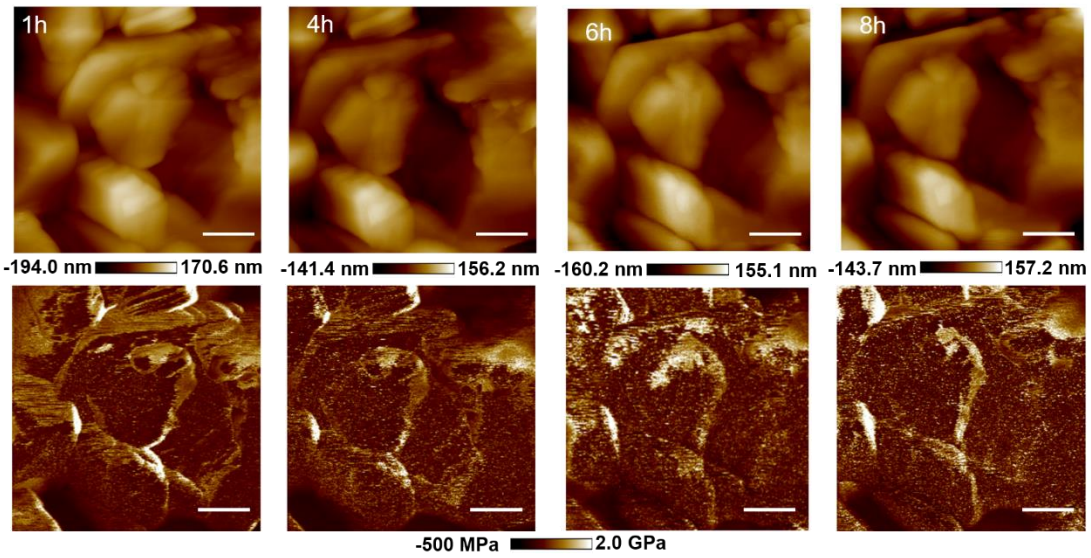

Figure S5. The AFM topography and DMT modulus mapping images of NCM523 electrode surface at OCP for 8 h. The scale bars are 300 nm.

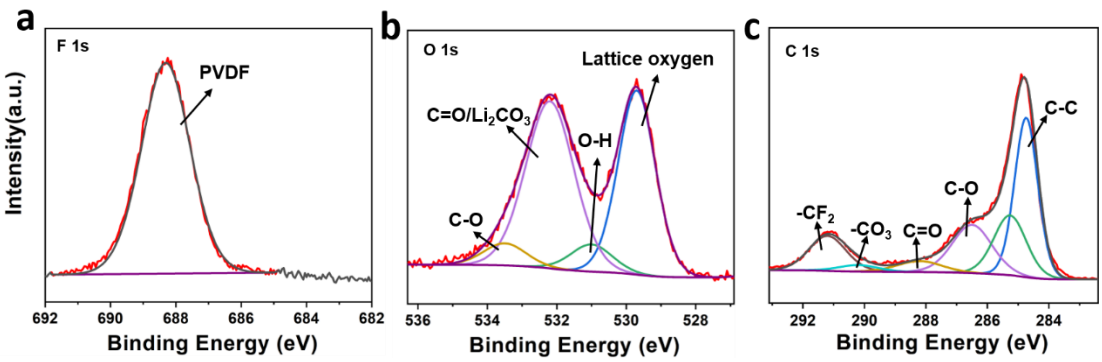

Figure S6. XPS (a) F 1s, (b) O 1s and (c) C 1s spectra of NCM523 electrode at OCP.

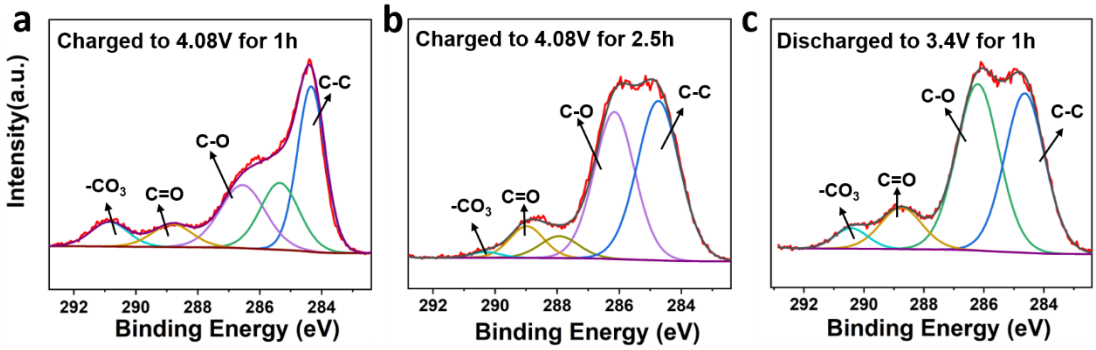

Figure S7. C 1s spectra of NCM523 electrode at different stages during the evolution of the cathode interphase at the first cycle. (a) Charged to 4.08 V for 1 h. (b) Charged to 4.08 V for 2.5 h. (c) Discharged to 3.4 V for 1 h.

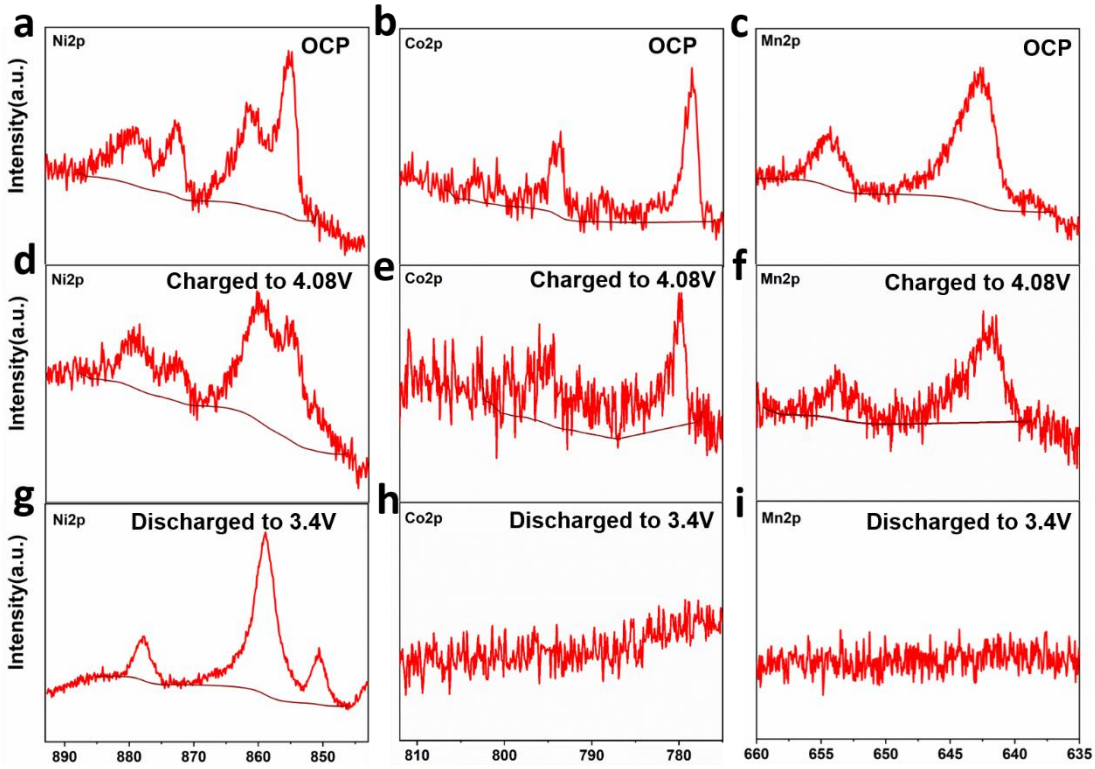

Figure S8. Co 2p, Mn 2p and Ni 2p spectra of NCM523 electrode at different stages during evolution of the cathode interphase. (a) Ni 2p, (b) Co 2p and (c) Mn 2p spectra at the OCP. (d) Ni 2p, (e) Co 2p and (f) Mn 2p spectra when charged to 4.08 V for 2.5 h. (g) Ni 2p, (h) Co 2p and (i) Mn 2p spectra when discharged to 3.4 V for 1 h.

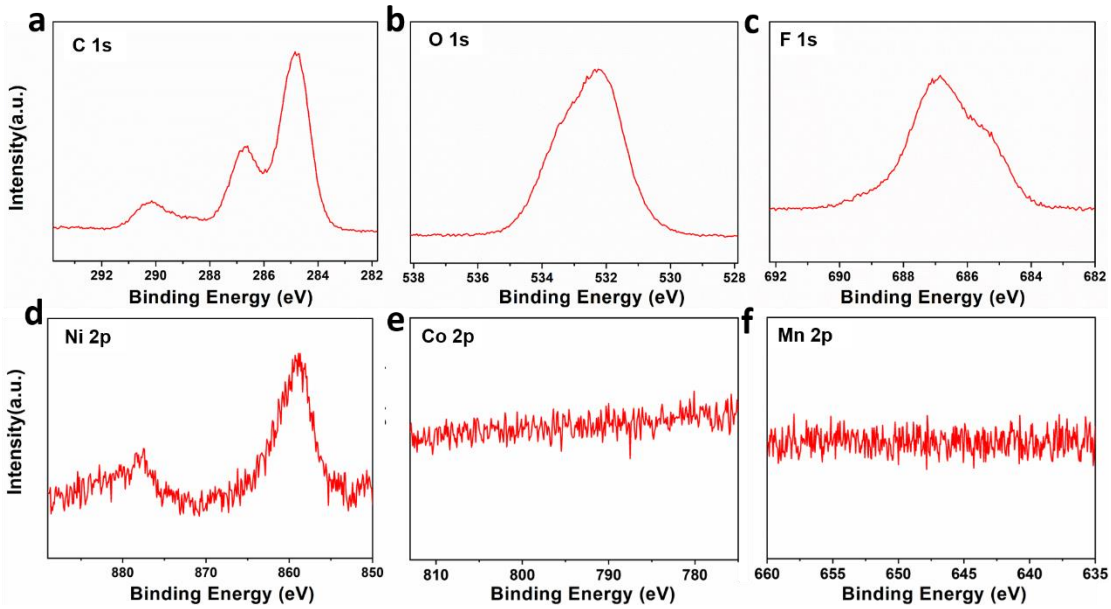

Figure S9. XPS (a) C1s, (b) O 1s, (c) F1s, (d) Ni 2p, (e) Co 2p, (f) Mn 2p spectra of Li anode surface at discharged to 3.4 V for 1h.

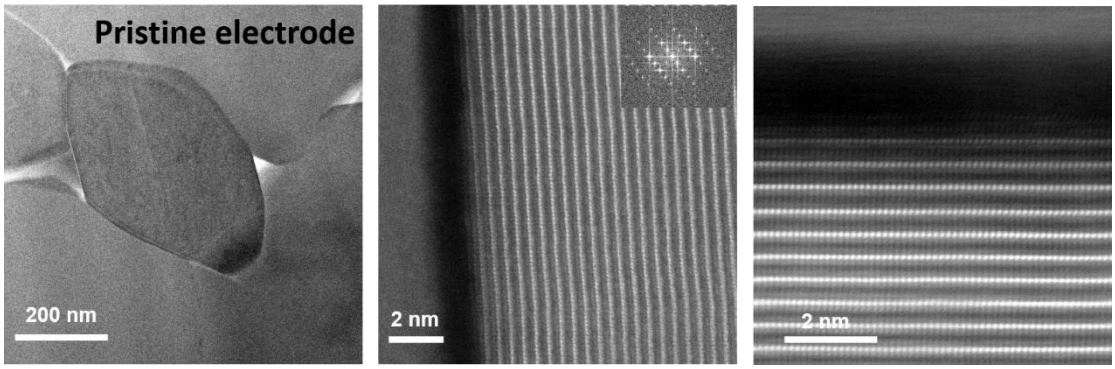

Figure S10. HRTEM images of NCM523 particles at OCP.

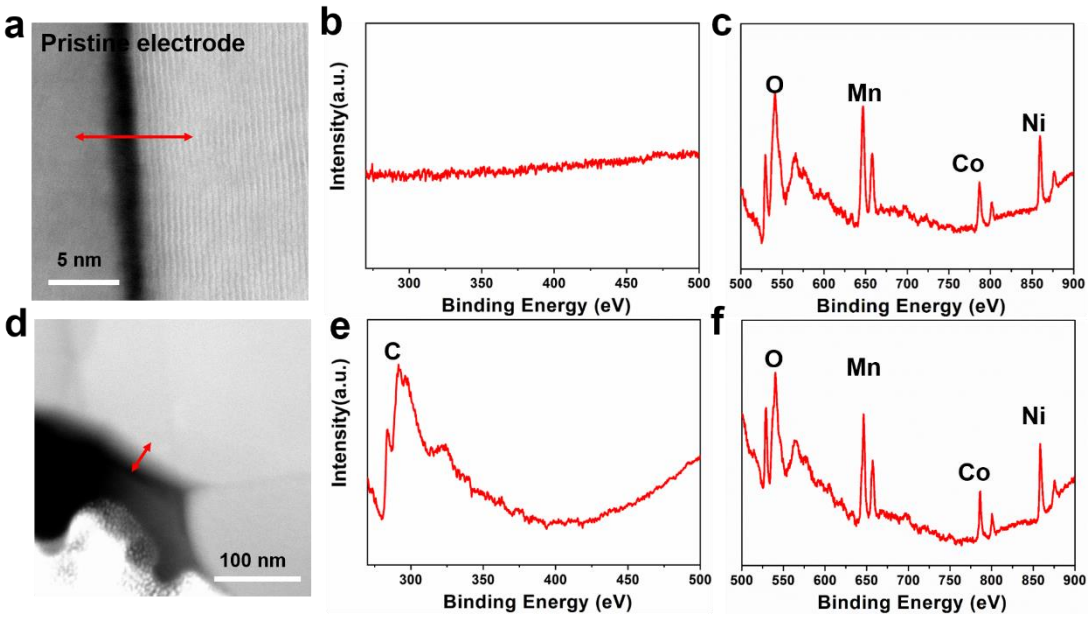

Figure S11. STEM-EELS spectra corresponding to the red line on the STEM images. (a) TEM image of pristine electrode. (b) Low-energy (275 ~ 500 eV) STEM-EELS spectra corresponding to the red arrow in (a). (c) High-energy (500 ~ 900 eV) STEM-EELS spectra corresponding to the red arrow in (a). (d) TEM image of NCM523 electrode after one cycle. (e) Low-energy (275 ~ 500 eV) STEM-EELS spectra corresponding to the red arrow in (d). (f) High-energy (500 ~ 900 eV) STEM-EELS spectra corresponding to the red arrow in (d).

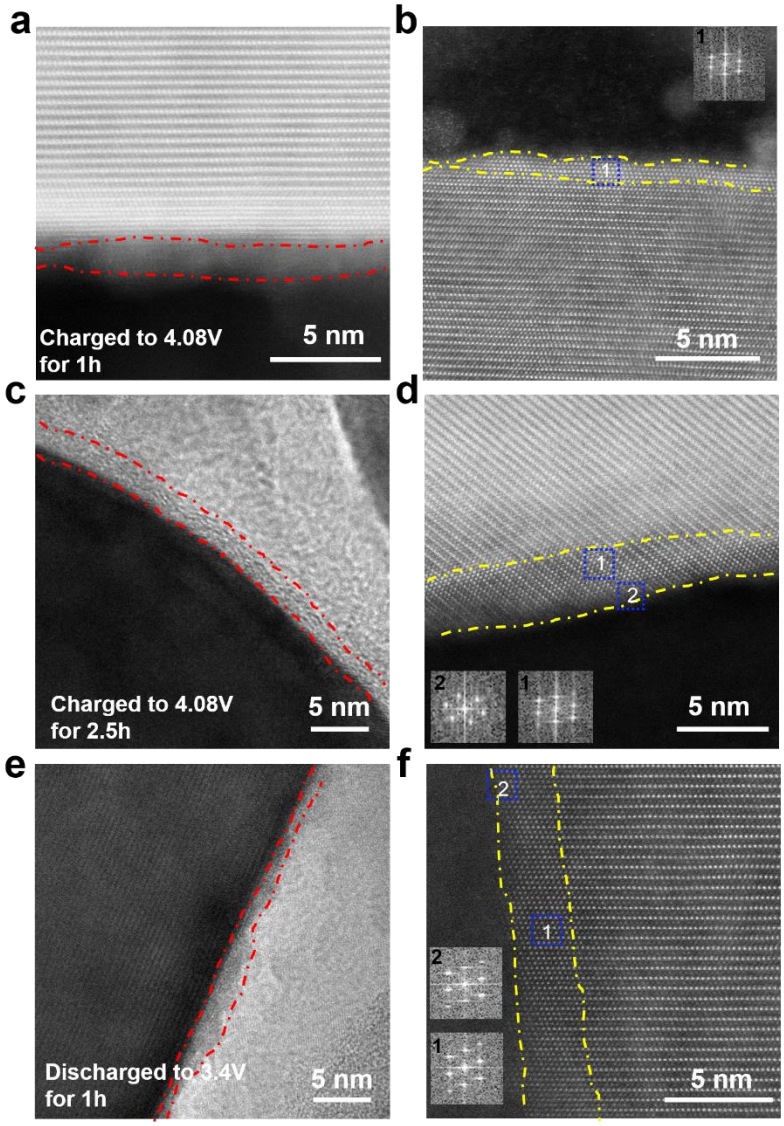

Figure S12. TEM images of NCM523 cathode surface at different stages. (a-b) Charged to 4.08 V for 1 h. (c-d) Charged to 4.08 V for 2.5 h. (e-f) Discharged to 3.4 V for 1 h. Insets in (b), (d), (f) corresponding to the fast Fourier transformation images of regions 1 and 2.

The detailed results of NCM523 electrode at different stages by HRTEM were provided in Figure S12. When the cell is charged to 4.08 V for 1 h, a thin amorphous layer (Figure S12a) and spinel phase (Figure S12b(1)) were observed in the narrow region ~1-2 nm on the NCM523 electrode surface (Figure S12b). At charging to 4.08 V for 2.5 h, a distinct amorphous layer with thickness of ~4-5 nm was observed on NCM523 surface (Figure S12c), as well as the phase transitions from rhombohedral phase to spinel phase (Figure S12d(1)) and rock-salt phase (Figure S12d(2)) occur on grain boundary of NCM523 particles (Figure S12d). When the cell is discharged to 3.4 V for 1 h, the amorphous layer remains with the thickness of ~4-5 nm (Figure S12e), along with the phase transformation from rhombohedral phase to spinel phase (Figure S12f(1)) and rock-salt (Figure S12f(2)) occurring on grain boundaries (Figure S12f).

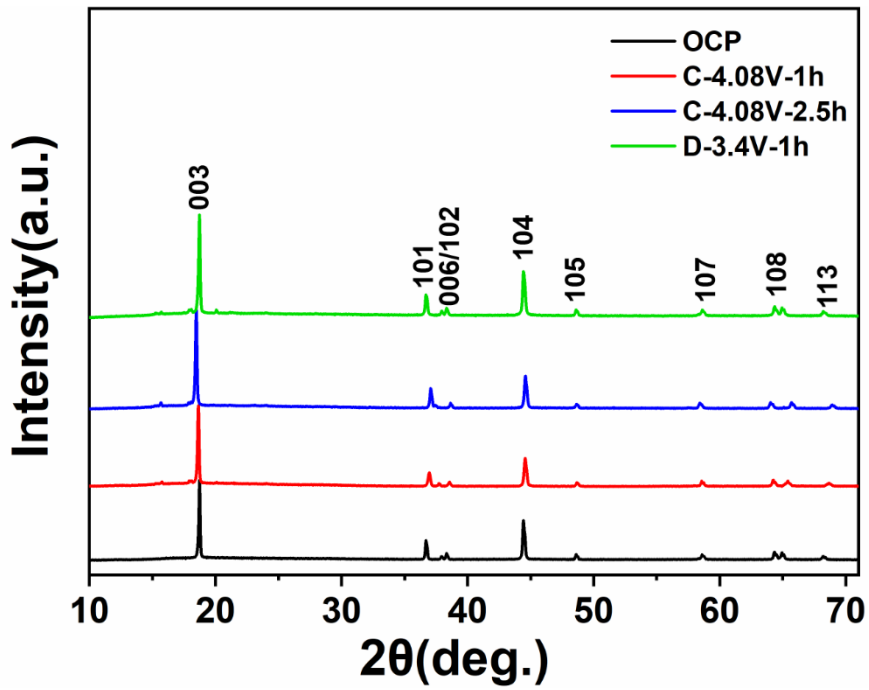

Figure S13. XRD data of NCM523 electrode at OCP, charged to 4.08 V for 1 h (C-4.08V-1h), charged to 4.08 V for 2.5 h (C-4.08V-2.5h), discharged to 3.4 V for 1 h (C-4.08V-2.5h).

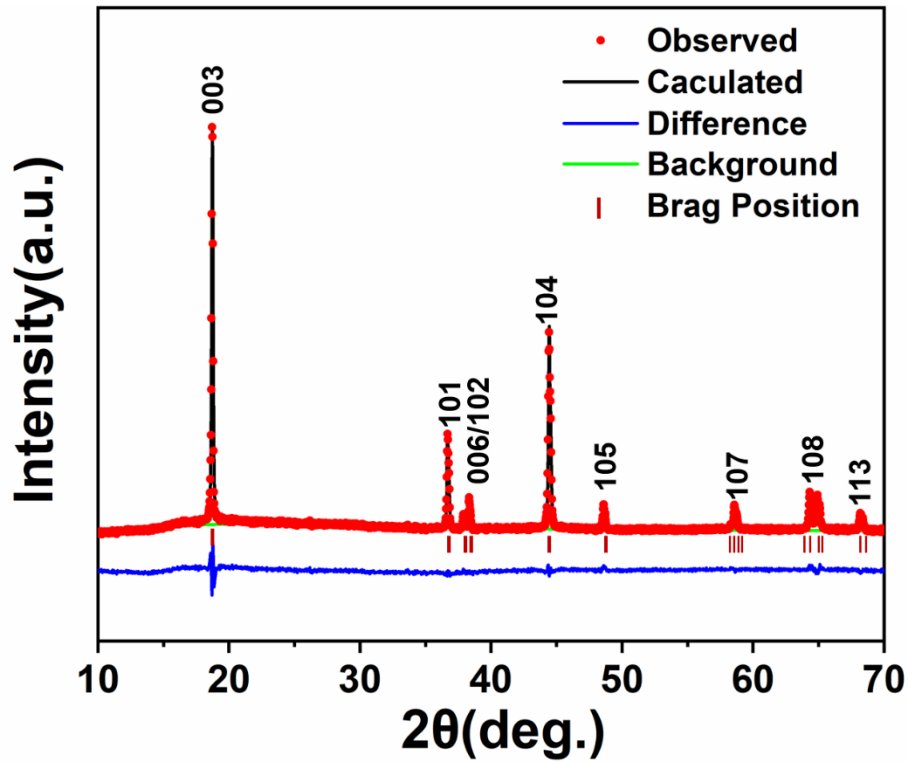

Figure S14. XRD patterns of $LiNi_{0.5}Co_{0.2}Mn_{0.3}O_2$ based on the R $\bar{3}$m. The R factors are Rp = 2.76%, Rwp = 3.52%.

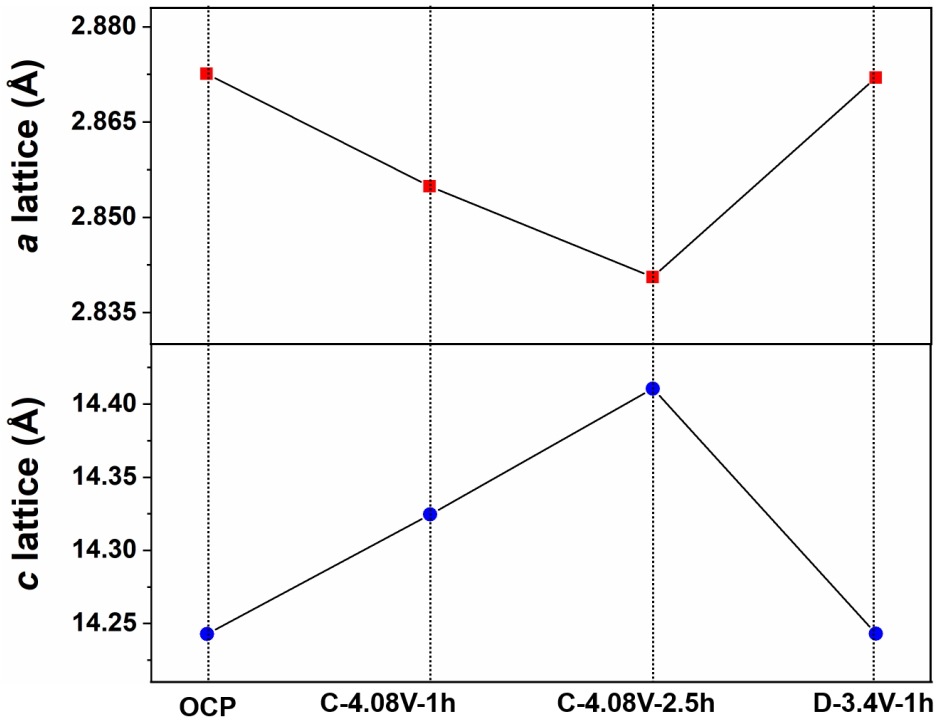

Figure S15. Lattice parameter changes of the electrodes at different stages obtained from Figure S13.

The refinement of the lattice parameters of the samples reveals that the "*a*" lattice parameter decreases, and the "*c*" lattice parameter increases with increasing charge time when compared to those at OCP. When the samples are discharged to 3.4 V for 1 h, the "*a*" lattice parameter increases, and the "*c*" lattice parameter decreases when compared to the sample after charge. Continuous change of the lattice parameters is mainly caused by the different amounts of remaining Li atom in each sample. The decrease of "*a*" lattice parameter is due to the smaller ionic radius upon the oxidation of the transition metal. In contrast, the "*c*" lattice parameter increases because the Li deficient state creates a stronger electrostatic repulsion between the two opposing oxygen layers across the Van der Waals gap.[1]

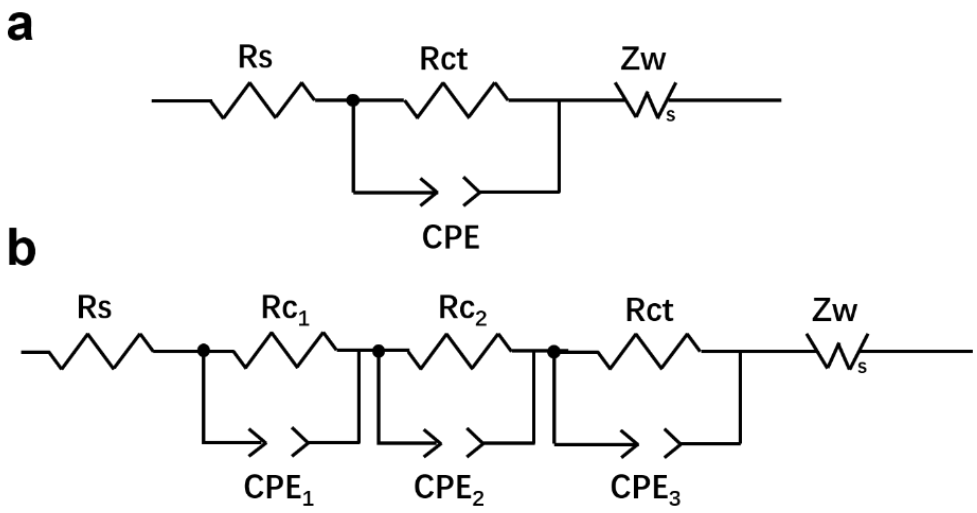

Figure S16. Equivalent circuits used to fit the impedance spectra of Figure 4f. (a) OCP. (b) Charged to 4.08 V for 1h, charged to 4.08 V for 2.5h and discharged to 3.4 V for 1h.

Equivalent circuits simulated to fit the experimental data are presented in Figure S16. Rs is the bulk resistance, Rct represents the charge transfer resistance, Rc_1 and Rc_2 are the resistance of cathode interphase layer. CPE is the constant phase element used instead of capacitance (Figure S16).

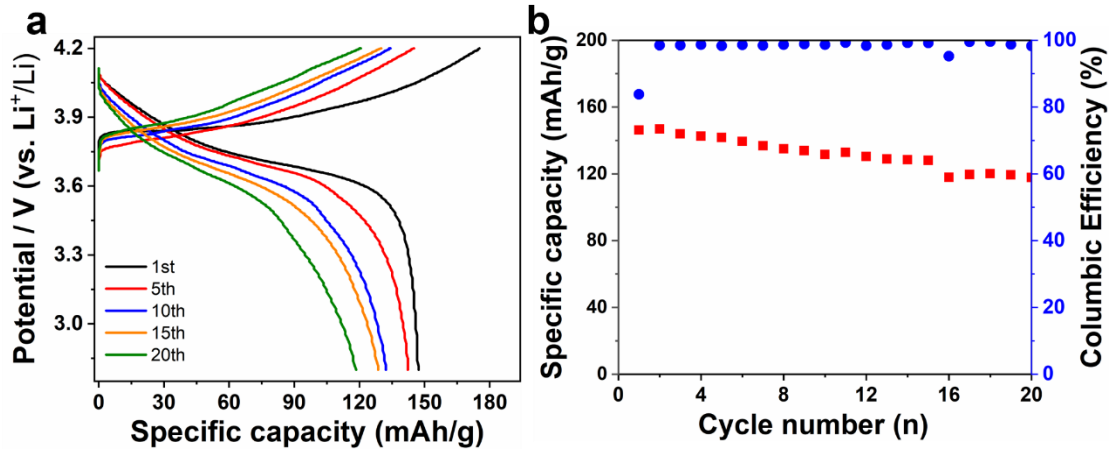

Figure S17. Electrochemical performance of NCM523/PEA/Li SSLB at a rate of 0.2 C. (a) Charge and discharge curves. (b) The specific capacity and Columbic efficiency during cycles.

To further evaluate the role of cathode interphase layer in the electrochemical process, the charge and discharge curves and cycling performances of NCM523/PEA/Li SSB at a rate of 0.2C between 2.8 and 4.2 V were provided in Figure S17. The initial discharge capacity is 147.3 mA h g^{-1} and the Columbic efficiency is 83.77 % at the first cycle. The lower discharge specific capacity and Columbic efficiency at the first cycle is mainly caused by the formation of cathode interphase layer. The Columbic efficiency increases to 98.5%, and the discharge specific capacity is 148.0 mA h g^{-1} at the second cycle when the cathode interphase becomes relatively stable on NCM 523 surface. The capacity retention over 20 cycles is 80.3% (118.4 mA h g^{-1}), and the Columbic efficiency at the 20th cycle is 98.3%. It is indicated that the cathode interphase layer has significant impact on the electrochemical behavior of SSLBs. A relatively stable cathode interphase layer would help to improve the electrochemical performance of the SSLBs.

Supplementary Tables

Table S1. Measurements of the thickness of cathode interphase layer.

AFM Measurement results	
No.	thickness of cathode interphase (nm)
1	4.11
2	5.03
3	5.03
4	5.05
5	5.44
6	5.79
7	6.04
8	6.06
9	6.51
10	6.61
11	6.94
12	7.07
13	7.12
14	7.85
15	8.04
16	8.10
17	8.12
18	8.17
19	8.45
20	8.62
21	8.91
22	9.46
23	9.52
24	10.14
25	10.52
26	10.74
27	10.82
28	10.83
29	11.03
30	11.16
31	11.19
32	11.36
33	12.13
34	12.39
35	12.73
36	12.84

37	13.39
38	13.52
39	14.39
40	14.72
41	14.93
42	14.96
43	16.07
44	16.77
45	17.52
46	17.66
47	21.83
48	21.84
49	21.97
50	29.44
Average	**11.18**
Stdeva	**4.48**

Table S2. The assignments of peaks on XPS F 1s, O1s and C 1s spectra.

Binding Energy (eV)	Peak	Assignment	Ref.
~529.7 eV	O 1s	Lattice oxygen	2-3
~531.0 eV		O-H	3-4
~532.0 eV		C=O/Li_2CO_3	4-5
~533.5 eV		C-O	2-3
~685.5 eV	F 1s	LiF	3, 5
~686.6 eV		$Li_xPF_yO_z$	5-6
~688.0 eV		CF_2 in PVDF	6
~284.8 eV	C 1s	C-C/C-H	5
~286.2 eV		C-O	3, 6
~287.9 eV		C=O	2, 5
~290.2 eV		-CO_3	2, 4

Table S3. The quantified chemical composition of cathode interphase on NCM523 surface at different stages as measured by XPS.

States	Components (%)									
	Ni	**Co**	**Mn**	**C=O/ Li_2CO_3**	**LiF**	**C-O**	**O-H**	**Lattice oxygen**	**PVDF**	**$Li_xPF_YO_z$**
Charged to 4.08V for 1h	4.81	0.62	1.05	14.24	37	5.55	4.55	4.85	22.9	4.43
Charged to 4.08V for 2.5h	3.25	0.55	0.71	14.76	3.46	29.5	16.52	3.25	17.28	10.72
Discharged to 3.4V	2.92	0.27	0.15	18.95	20.1	17.25	2.46	0.02	14.78	23.1

Table S4. Lattice parameters of NCM523 electrode at different stages of Figure S13.

	a **(Å)**	***c*** **(Å)**
OCP	2.8726	14.2427
Charged to 4.08V for 1h	2.8529	14.3245
Charged to 4.08V for 2.5h	2.8406	14.4105
Discharged to 3.4V for 1h	2.8720	14.2430

Table S5. Resistance values obtained from EIS spectra in Figure 4f fitted by the equivalent circuits in Figure S16.

	Rs (Ω)	**Rc_1 (Ω)**	**Rc_2 (Ω)**	**Rct (Ω)**
OCP	11.8	/	/	3760
Charged to 4.08V for 1h	7.89	7.57	6.73	9.40
Charged to 4.08V for 2.5h	6.08	7.75	7.04	26.0
Discharged to 3.4V for 1h	8.55	11.9	20.1	180

Supplementary References

1. Jung, S.-K.; Gwon, H.; Hong, J.; Park, K.-Y.; Seo, D.-H.; Kim, H.; Hyun, J.; Yang, W.; Kang, K., Understanding the Degradation Mechanisms of $LiNi_{0.5}Co_{0.2}Mn_{0.3}O_2$ Cathode Material in Lithium Ion Batteries. Advanced Energy Materials 2014, 4 (1), 1300787.
2. Zhang, J.-N.; Li, Q.; Ouyang, C.; Yu, X.; Ge, M.; Huang, X.; Hu, E.; Ma, C.; Li, S.; Xiao, R.; Yang, W.; Chu, Y.; Liu, Y.; Yu, H.; Yang, X.-Q.; Huang, X.; Chen, L.; Li, H., Trace doping of multiple elements enables stable battery cycling of $LiCoO_2$ at 4.6 V. *Nature Energy* **2019,** *4* (7), 594-603.
3. Verdier, S.; El Ouatani, L.; Dedryvère, R.; Bonhomme, F.; Biensan, P.; Gonbeau, D., XPS Study on Al_2O_3- and $AlPO_4$- Coated $LiCoO_2$ Cathode Material for High-Capacity Li Ion Batteries. *Journal of The Electrochemical Society* **2007,** *154* (12), A1088.
4. Zhang, J.-N.; Li, Q.; Wang, Y.; Zheng, J.; Yu, X.; Li, H., Dynamic evolution of cathode electrolyte interphase (CEI) on high voltage $LiCoO_2$ cathode and its interaction with Li anode. *Energy Storage Materials* **2018,** *14*, 1-7.
5. Lu, Y. C.; Mansour, A. N.; Yabuuchi, N.; Shao-Horn, Y., Probing the Origin of Enhanced Stability of "$AlPO_4$ " Nanoparticle Coated $LiCoO_2$ during Cycling to High Voltages: Combined XRD and XPS Studies. *Chemistry of Materials* **2009,** *21* (19), 4408-4424.
6. Yang, Q.; Wang, W.; Qian, K.; Li, B., Investigation of Interfacial Changes on Grain Boundaries of $Li(Ni_{0.5}Co_{0.2}Mn_{0.3})O_2$ in the Initial Overcharge Process. *Advanced Materials Interfaces* **2019,** *6* (6), 1801764.